SCEC Project 20199 – Final Technical Report

Modeling the Rupture Dynamics of Strong Ground Acceleration (>1g) in Fault Stepovers

Julian Lozos (California State University, Northridge)
Sinan Akçiz (California State University, Fullerton)

Introduction

Following the July 2019 Ridgecrest earthquakes, multiple field investigators noted that pebble- to boulder-sized rocks had been displaced from their place in the desert pavement within an extensional stepover toward the southern end of the right-lateral strike-slip M7.1 rupture trace (Akçiz et al., 2019; Sleep and Hough, 2020). There were no drag marks between the rocks' new locations and the imprints of their previous places in the ground, and some were clearly flipped upside down, suggesting that they may have been tossed out of place, not dragged or sheared. The implication here is that the Ridgecrest earthquake produced localized ground accelerations in excess of 1 g – a value which contrasts the observational maximum of ~0.5 g (Hough et al., 2020). We also introduce previously-unpublished observations of displaced rocks concentrated in stepovers in the predominantly right-lateral strike-slip 2010 M7.2 El Mayor-Cucapah earthquake. Because these rocks were concentrated only at fault discontinuities and stepovers, they suggest that something about how earthquake rupture negotiates discontinuous strike-slip faults produces extremely localized strong ground accelerations.

The question of how fault stepovers control ground motion distribution and intensity is not new, even if these observations of displaced rocks are relatively recent. Direct recordings of strong motions within fault stepovers have been limited by the layout of a seismic network relative to the source fault. However, previous modeling studies show high ground velocities within stepovers. Lozos et al. (2013) conducted dynamic rupture simulations across disconnected stepovers in a variety of material settings, and found that subshear ruptures produce a stopping phase from the rupture front hitting the end of the first fault that causes high peak ground velocity (PGV) within the stepover. They did not see this effect for supershear ruptures. However, their work only covers low frequency < 1 Hz velocities, and does not address peak ground acceleration (PGA). Hu et al. (2018) used kinematic simulations to address the question of ground motion in both disconnected and connected stepovers at higher frequency content, and in contrast, found that supershear ruptures in particular incite strong high-frequency shaking within the stepover region.

These observations and past simulations alike imply that the areas within and immediately adjacent to fault stepovers may have particularly high ground shaking hazard, even compared to areas only a small distance away along the same faults. Here, we use dynamic rupture simulations to investigate the mechanism behind strong ground acceleration in strike-slip stepovers, and how the specific geometry of the stepover may affect the intensity and location of the strongest shaking.

Methods

We use the 3D finite element software FaultMod (Barall, 2009), which has performed consistently in the USGS Dynamic Rupture Code Verification Exercise (Harris et al., 2009; Harris et al., 2018), to investigate how dynamic rupture across stepovers in strike-slip faults may generate strong ground accelerations. Fault geometry is our primary variable. We model two planar, vertical strike-slip faults with 12 km basal depth: one 30 km long, separated from a stepover of variable geometry from a 10 km-long fault. The stepover width varies between 1 and 5 km in either the compressional or the extensional direction; and the horizontal distance between the strands between 5 km overlap to 5 km separation. We mesh these geometries directly within FaultMod. Our mesh discretization allows us to assess PGA at frequencies up to 5 Hz. Because we want to isolate how a geometrically-complex earthquake source controls shaking, without significant path or site effects, we parameterize the area around the faults as a homogeneous, fully-elastic half space.

We also assign homogeneous initial tractions to both faults to help isolate geometrical effects. For each of our model geometries, we test two different initial stress conditions: one of which produces subshear rupture velocity and the other of which produces supershear ruptures. The specific stress values for our two main cases come from other dynamic rupture modeling geometrical parameter studies (e.g., Harris and Day, 1993; Lozos et al., 2013), so our current study can be directly compared with this previous work. In all cases, we use linear slip-weakening friction (Ida, 1972; Andrews, 1976), and we begin the rupture at the end of the longer fault furthest from the stepover by raising the shear stress over the yield stress over an area larger than the critical patch size required for self-sustaining rupture (Day, 1982).

Results

Rupture Behavior

Our models produced four rupture behaviors:

1. Rupture jumps the stepover and propagates completely through both faults (“complete rupture”).
2. Rupture jumps the stepover and propagates through the parts of the second fault that do not overlap with the first fault (“partial rupture”).
3. Rupture propagates through the first fault, but only produces a small patch of triggered slip on the second fault (“triggered slip).
4. Rupture is unable to jump the stepover in any form, resulting in only the first fault slipping (“no slip”).

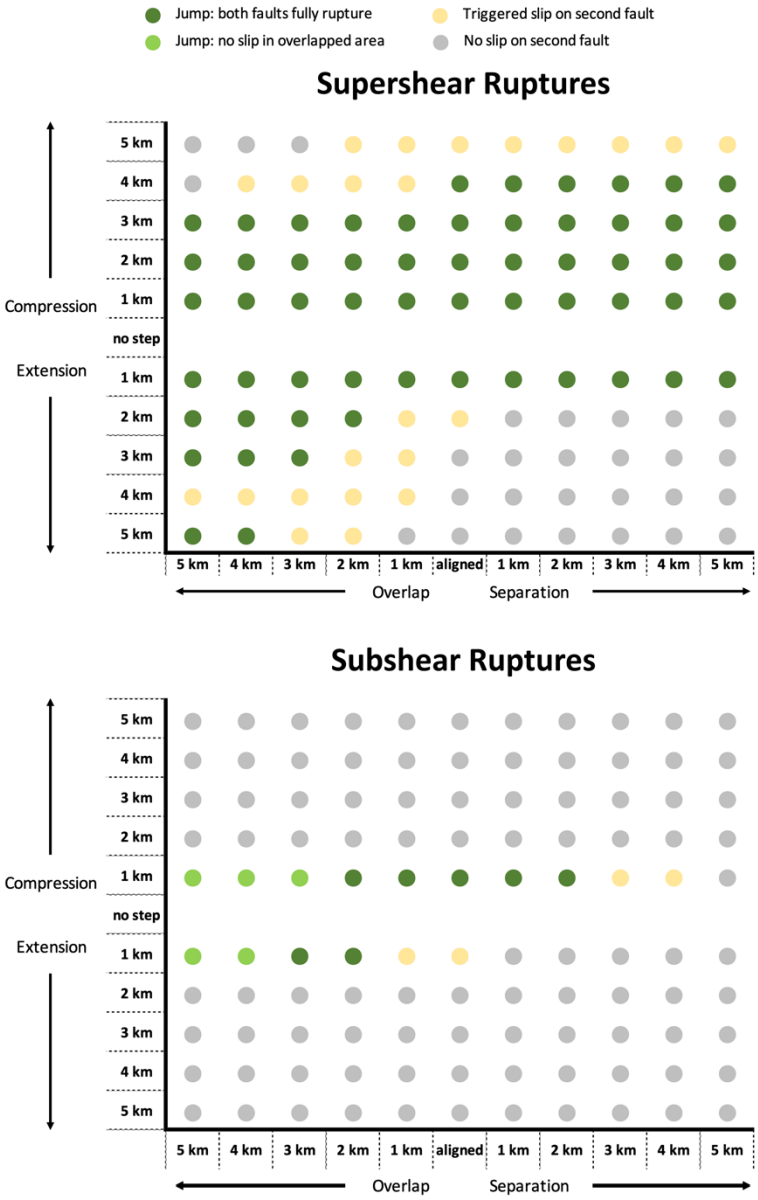

Figure 1. Rupture behaviors across our entire parameter space. Each dot represents a single simulation.

Figure 1 shows which rupture behaviors occurred on which geometries for our entire parameter space. Our results for which fault geometries allow versus prohibit jumping rupture are extremely consistent with the ˜5 km separation cutoff determined both from previous modeling studies (e.g., Harris and Day, 1993; Oglesby, 2008; Lozos et al., 2013) and from empirical analysis of surface ruptures (e.g., Wesnousky, 2008; Biasi and Wesnousky, 2016). We also found that overlapping geometries allow rupture to jump larger stepover widths for extensional cases, and separated geometries allow larger jumps in compressional cases. This is consistent with the pattern of stress changes caused by rupture hitting the end of the first fault (e.g., Harris and Day, 1993; Duan and Oglesby, 2006; Lozos et al., 2015): the separated case places the second fault within the lobe of increased shear stress to the compressional side of the first fault, and the second fault in the overlapping case intersects the lobe of increased shear stress to the extensional side.

Ground Motion

The details of the stepover geometry – whether extension versus compression, overlapping versus separated, small or wide stepover distance – had a negligible effect on the ground motions generated by our simulations. Figure 2 shows maximum horizontal and vertical particle accelerations across our full parameter space. For our subshear rupture cases, there were very small fluctuations in maxima, associated with whether or

not rupture jumped the stepover. For our supershear case, however, ground motion maxima were exactly the same across the entirety of the parameter space, regardless of any geometrical variation.

For both our subshear and supershear rupture velocity cases, all peak horizontal particle velocities were larger than 1 g, but peak vertical particle velocities were still under 1 g. The fact that the horizontal ground motions were stronger is consistent with the behavior of pure strike-slip faults with no vertical slip. The exact ground motion intensities in these simulations are direct results of our specific arbitrary stress cases that we chose, but we still note that the subshear case produced consistently stronger horizontal and vertical ground motions across our parameter space than the supershear case did. This is a particularly intriguing result given that both the El Mayor-Cucapah (Wei et al., 2011) and Ridgecrest (Liu et al., 2019; Wang et al., 2020) earthquakes, with their displaced rocks, had very slow rupture velocities.

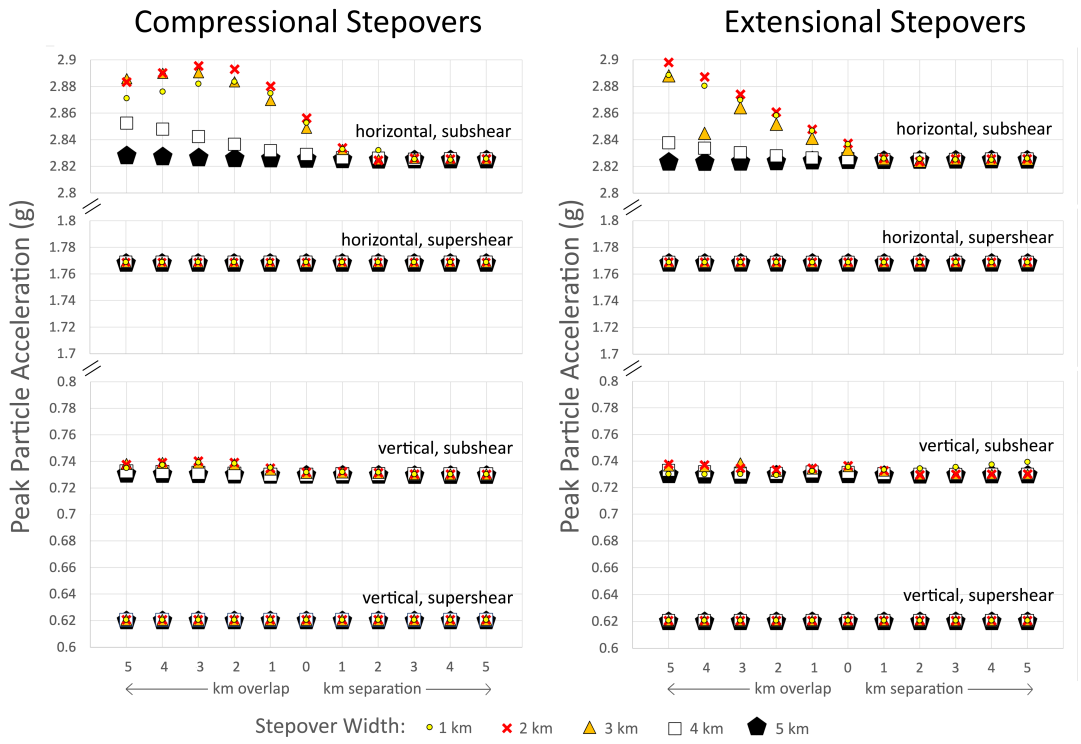

Figure 2. Peak horizontal and vertical particle accelerations (G) for all of our simulations. Note the breaks in the Y-axis. We had to use Y-axis increments of only 0.02 G to show what little variation there was between these models.

Discussion

Why Specific Stepover Geometry Does Not Matter

We did not expect that the details of the stepover geometry would have such a small effect maximum ground motions. The presence of a stepover at all, regardless of its dimensions, is what had a controlling effect.

Figure 3 (left) shows a plot of peak particle accelerations for an example subshear rupture; here, the strongest shaking occurs when rupture reaches the end of the first fault. As the rupture front propagates along the first fault, it grows in energy due to directivity, in which shear stress carried by seismic waves propagating ahead of the rupture front feeds into the rupture itself (e.g., Ben-Menahem, 1961). An energetic rupture hitting a geometrical discontinuity on a fault (whether a break or a bend) produces a high-energy stopping phase: an effect which is described in other modeling studies (e.g., Madariaga, 1977; Harris and Day, 1993; Oglesby, 2008; Lozos et al., 2011) and observational analyses (e.g., Savage, 1965; Brüstle and Müller, 1977; Imanishi et al., 2004) alike. A rupture front inherently cannot propagate beyond the end of the fault; a small amount of the energy in the stopping phase goes into fracturing unbroken rock, but most of it goes into wave propagation and shaking (Kanamori and Rivera, 2006). Because this stopping phase comes from rupture on the first fault, it occurs regardless of the position of the second fault. Particle accelerations are slightly lower in ruptures that do jump the

stepover because some energy from the stopping phase goes into re-nucleation rather than just shaking, but the variation is less than 0.1 g.

Figure 3 (right) also shows peak particle accelerations for a supershear rupture on the same fault geometry. Here, the strongest shaking is associated with the supershear transition, partway along the first fault. This is well before the rupture front reaches the stepover region; therefore, the specific stepover geometry is irrelevant. The process of supershear rupture is effectively a jumping rupture in and of itself: the shear stress perturbation ahead of the rupture front is large enough that a secondary rupture front forms ahead of the shear wave front, and the original subshear front slowly dies out (e.g., Dunham et al., 2006; Bruhat et al., 2016). This effect is caused by directivity, but the supershear transition is also effectively a break in directivity even along a planar fault, since the shear stress high ahead of the original subshear rupture front is used up by nucleating the supershear one. Therefore, the strongest shaking in the supershear models occurs right before the transition point. There is still a stopping phase effect at the end of the first fault in the supershear models, but it is weaker than in the subshear models.

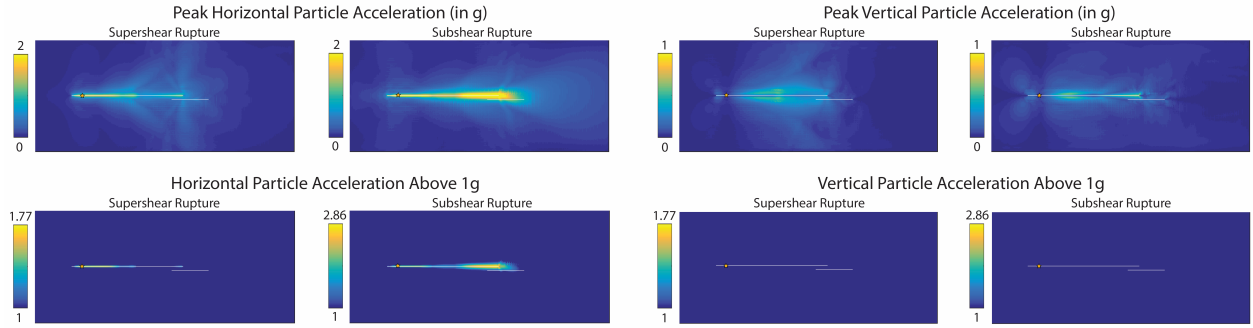

Figure 3. Map-view plots of peak ground acceleration (PGA) for an extensional stepover with 1 km separation and 2 km overlap. The top row of plots shows the overall pattern of vertical and horizontal shaking from supershear and subshear rupture on this model geometry. Shaking extends further from the fault in the supershear cases, but is stronger in the subshear cases. The bottom set of panels highlights only where PGA in excess of 1 g occurred. For both subshear and supershear cases, the strongest motion was immediately adjacent to the fault; the peak occurred at the point of supershear transition for the supershear models, and at the end of the first fault for the subshear models.

Our specific, arbitrary choice of fault size likely affects the exact locations of the strongest shaking. We expect that a sustained supershear rupture on a longer fault might have a stronger stopping phase effect at the end of the first fault due to rupture directivity building back up; however, a subshear rupture on the same longer fault would produce stronger shaking still, due to not needing to reestablish its directivity effect after a supershear transition. Similarly, we expect that the stopping phase effect at the end of the second fault, in ruptures that jumped the stepover, would be larger if the fault were longer. Regardless, this effect is independent of the specific dimensions of the stepover.

Why Subshear Ruptures Shake Harder

Sustained versus broken directivity is only part of why our subshear ruptures produce stronger shaking than supershear ones do. The energy budget of the rupture also plays a role. The energy in a rupture front is divided between crack propagation, seismic radiation, and fracturing new rock (Kanamori and Rivera, 2006). Most of that budget goes toward rupture front propagation in supershear ruptures, leaving less energy for strong seismic radiation (Kanamori and Rivera, 2006; Okubo et al., 2019). In contrast, because subshear ruptures are inherently slower, more of their energy can go into producing strong seismic waves.

A third key aspect is the difference between static and dynamic stress drop for our subshear versus supershear cases. Within slip-weakening friction, static stress drop refers to the difference in shear stress before and after the rupture (Ida, 1972; Andrews, 1976; Day, 1982); all of our stress/rupture velocity cases have the same 6 MPa static stress drop. Dynamic stress drop, however, is the difference between the maximum shear stress carried by the rupture front during the earthquake and the final post-rupture shear stress (Boatwright, 1980).

In order for rupture to propagate, the shear stress must exceed the yield stress, defined as the normal stress multiplied by the static coefficient of friction (Ida, 1972; Andrews, 1976). Our static coefficients of friction are the same for our primary subshear and supershear stress cases. In our subshear models, the higher normal stress means that the yield stress required for initiating rupture also must be higher than in our supershear case. The difference between shear pre-stress and yield stress is therefore also higher for our subshear models than our supershear ones. This means that the total shear stress in the rupture front, and the dynamic stress drop, is higher for our subshear models than the supershear ones. Observational seismology shows that higher dynamic stress drops are associated with stronger shaking (e.g., Hanks and McGuire, 1981; Baltay et al., 2013; Oth et al., 2017). Our results are consistent with these observations, as well as with other dynamic rupture modeling studies addressing ground motion intensity (e.g., Guatteri et al., 2003; Lozos et al., 2013; Shi and Day, 2013).

Implications for Displaced Rocks

Our simulations constitute a parameter study in a very simplified material and stress setting. None of our models are tailored to match the specific conditions of either the 2010 El Mayor-Cucapah or the 2019 Ridgecrest earthquakes, neither in terms of fault geometry nor stresses. That said, the ground motion patterns we see in our simulations are consistent with observations from these two earthquakes. The displaced rocks in both earthquakes were aligned with the end of one fault segment, and were in line with the rupture directivity (Akçiz et al., 2019; Zuckerman et al., 2019). This suggests that a stopping phase could have produced local strong shaking in the areas where the rocks were found. Additionally, both the El Mayor-Cucapah and Ridgecrest earthquakes had slow rupture velocities (Wei et al., 2011; Liu et al., 2019; Wang et al., 2020), consistent with our subshear models producing stronger ground motions.

The fact that our models produce the strongest accelerations in the horizontal direction is consistent with the placement of the displaced rocks outside of and horizontally offset from their indentations. Even though our vertical ground motions are less than 1 g, the combined acceleration vector still exceeds 1 g. This could be enough to produce predominantly horizontal rock displacement without leaving drag marks.

We note again that all of our > 1 g ground motions occurred within 1 km of the source fault, and that peak particle accelerations rapidly tapered down to below 1 g past this distance. This implies that the strongest motions may not be captured by a seismic station unless its pre-event placement was extremely lucky. Thus, > 1 g, rock-displacing ground motions are not inherently a contradiction with observational maxima below 1 g. While it is unrealistic to suggest densely instrumenting all hazardous fault stepovers in hopes of recording this level of shaking, we do still suggest that localized extremely strong shaking around stepovers should be taken into account in seismic hazard assessments. We also suggest that finding similarly displaced rocks or other objects in the extreme near field to the source fault can be indicative of localized extreme strong motion, to the point where preserved displaced features may even be useful for determining or constraining ground motion intensities from pre-instrumental earthquakes.

Conclusions

We simulated dynamic ruptures across a wide range of strike-slip stepover geometries, and found that rupture reaching the end of one fault, whether or not it re-nucleates on the next, can cause localized ground accelerations in excess of 1 g. The specific geometry of the stepover does not matter here; the discontinuity in general causes this effect. Other effects that break rupture directivity (in the sense of the rupture front and the waves released ahead of it becoming misaligned), such as fault bends, or even supershear transitions on a planar fault, can produce similar localized acceleration spikes. We also find that a narrow zone of shaking in excess of 1 g can occur within the several hundred meters closest to even a straight, continuous fault segment. Even the larger areas of PGA > 1 g associated with breaks in directivity are limited to within 1 km of our model faults. In real world ruptures, site conditions may affect the intensity and range of these stronger motions; however, this would likely still be enough of a near-field effect to not be captured by seismic networks, leading to an apparent mismatch between recorded PGA and the PGA implied by the displaced objects. This suggests that ground motion predictions and local hazard assessments should account for much stronger shaking in the immediate near field of active faults, especially around stepovers and other geometrical discontinuities. Crude strong motion data from displaced boulder- or cobble-sized rocks (or other similarly large objects) observed near faults after earthquakes may be a useful dataset for refining the details of those ground motion predictions and hazard assessments.

Submitted Manuscript (SCEC Publication Database #13434)
Lozos, J. C., Akciz, S. O., & Ladage, H. (2023). Modeling the rupture dynamics of strong ground motion (> 1 g) in fault stepovers. *Tectonophysics*, (under review).

References Cited

Akciz, S. O., Padilla, S., Hatem, A. E., & Dolan, J. F. (2019, December). Fault slip distribution and structural style along the southern 15 km of the M7. 1 Ridgecrest earthquake surface rupture: Initial observations. In *AGU Fall Meeting Abstracts* (Vol. 2019, pp. S34C-04).

Andrews, D. J. (1976). Rupture propagation with finite stress in antiplane strain. *Journal of Geophysical Research*, *81*(20), 3575-3582.

Baltay, A. S., Hanks, T. C., & Beroza, G. C. (2013). Stable stress-drop measurements and their variability: Implications for ground-motion prediction. *Bulletin of the Seismological Society of America*, *103*(1), 211-222.

Barall, M. (2009). A grid-doubling finite-element technique for calculating dynamic three-dimensional spontaneous rupture on an earthquake fault. *Geophysical Journal International*, *178*(2), 845-859.

Ben-Menahem, A. (1961). Radiation of seismic surface-waves from finite moving sources. *Bulletin of the Seismological Society of America*, *51*(3), 401-435.

Biasi, G. P., & Wesnousky, S. G. (2016). Steps and gaps in ground ruptures: Empirical bounds on rupture propagation. *Bulletin of the Seismological Society of America*, *106*(3), 1110-1124.

Boatwright, J. (1980). A spectral theory for circular seismic sources; simple estimates of source dimension, dynamic stress drop, and radiated seismic energy. *Bulletin of the Seismological Society of America*, *70*(1), 1-27.

Bruhat, L., Fang, Z., & Dunham, E. M. (2016). Rupture complexity and the supershear transition on rough faults. *Journal of Geophysical Research: Solid Earth*, *121*(1), 210-224.

Brüstle, W., & Müller, G. (1987). Stopping phases in seismograms and the spatiotemporal extent of earthquakes. *Bulletin of the Seismological Society of America*, *77*(1), 47-68.

Das, S., & Aki, K. (1977). A numerical study of two-dimensional spontaneous rupture propagation. *Geophysical journal international*, *50*(3), 643-668.

Day, S. M. (1982). Three-dimensional simulation of spontaneous rupture: the effect of nonuniform prestress. *Bulletin of the Seismological Society of America*, *72*(6A), 1881-1902.

Duan, B., & Oglesby, D. D. (2006). Heterogeneous fault stresses from previous earthquakes and the effect on dynamics of parallel strike-slip faults. *Journal of Geophysical Research: Solid Earth*, *111*(B5).

Dunham, E. M. (2007). Conditions governing the occurrence of supershear ruptures under slip-weakening friction. *Journal of Geophysical Research: Solid Earth*, *112*(B7).

DuRoss, C., Gold, R., Dawson, T., Scharer, K., Kendrick, K., Akciz, S. O., & Zinke, R. (2020). Surface Displacement Distributions for the July 2019 Ridgecrest, California, Earthquake Ruptures. *Bulletin of the Seismological Society of America*, doi:10.1785/0120200058.

Fletcher, J. M.,Teran, O. J., Rockwell, T. K., Oskin, M. E., Hudnut, K. W., Mueller, K. J., Spelz, R. M., Akciz, S. O., Masana, E., Faneros, G., Fielding, E. J., Leprince, S., Morelan, A. E., Stock, J., Lynch, D. K., Elliott, A. J., Gold, P., Liu-Zeng, J., González-Ortega, A., Hinojosa-Corona, A., & González-García, J. (2014). Assembly of a large earthquake from a complex fault system: Surface rupture kinematics of the 4 April 2010 El Mayor–Cucapah (Mexico) M_w 7.2 earthquake. *Geosphere*, v. 10, p. 797-827.

Guatteri, M., Mai, P. M., Beroza, G. C., & Boatwright, J. (2003). Strong ground-motion prediction from stochastic-dynamic source models. *Bulletin of the Seismological Society of America*, *93*(1), 301-313.

Hanks, T. C., & McGuire, R. K. (1981). The character of high-frequency strong ground motion. *Bulletin of the Seismological Society of America*, *71*(6), 2071-2095.

Harris, R. A., & Day, S. M. (1993). Dynamics of fault interaction: Parallel strike-slip faults. *Journal of Geophysical Research: Solid Earth*, *98*(B3), 4461-4472.

Harris, R. A., Barall, M., Archuleta, R., Dunham, E., Aagaard, B., Ampuero, J. P., Bhat, H., Cruz-Atienza, V., Dalguer, L., Dawson, P., Day, S., Duan, B., Ely, G., Kaneko, Y., Kase, Y., Lapusta, N., Liu, Y., Ma, S., Oglesby, D., Olsen, K., Pitarka, A., Song, S., & Templeton, E. (2009). The SCEC/USGS dynamic earthquake rupture code verification exercise. *Seismological Research Letters*, *80*(1), 119-126.

Harris, R. A., Barall, M., Aagaard, B., Ma, S., Roten, D., Olsen, K., Duan, B., Liu, D., Luo, B., Bai, K., Ampuero, J.-P., Kaneko, Y., Gabriel, A., Duru, K., Ulrich, T., Wollherr, S., Shi, Z., Dunham, E., Bydlon, S., Zhang, Z., Chen, X.,

Somala, S., Pelties, C., Tago, J., Cruz-Atienza, V., Kozdon, J., Daub, E., Aslam, K., Kase, Y., Withers, K., & Dalguer, L. (2018). A suite of exercises for verifying dynamic earthquake rupture codes. *Seismological Research Letters*, *89*(3), 1146-1162.

Hough, S. E., Thompson, E., Parker, G. A., Graves, R. W., Hudnut, K. W., Patton, J., Dawson, T., Ladinsky, T., Oskin, M., Sirorattanakul, K., Blake, K., Baltay, A., & Cochran, E. (2020). Near-field ground motions from the July 2019 Ridgecrest, California, earthquake sequence. *Seismological Research Letters*, *91*(3), 1542-1555.

Hu, F., Wen, J., & Chen, X. (2018). High frequency near-field ground motion excited by strike-slip step overs. *Journal of Geophysical Research: Solid Earth*, *123*(3), 2303-2317.

Ida, Y. (1972). Cohesive force across the tip of a longitudinal-shear crack and Griffith's specific surface energy. *Journal of Geophysical Research*, *77*(20), 3796-3805.

Imanishi, K., Takeo, M., Ellsworth, W. L., Ito, H., Matsuzawa, T., Kuwahara, Y., Iio, Y., Horiuchi, S., & Ohmi, S. (2004). Source parameters and rupture velocities of microearthquakes in Western Nagano, Japan, determined using stopping phases. *Bulletin of the Seismological Society of America*, *94*(5), 1762-1780.

Kanamori, H., & Rivera, L. (2006). Energy partitioning during an earthquake.

Liu, C., Lay, T., Brodsky, E. E., Dascher-Cousineau, K., & Xiong, X. (2019). Coseismic rupture process of the large 2019 Ridgecrest earthquakes from joint inversion of geodetic and seismological observations. *Geophysical Research Letters*, *46*(21), 11820-11829.

Lozos, J. C., Oglesby, D. D., & Brune, J. N. (2013). The effects of fault stepovers on ground motion. *Bulletin of the Seismological Society of America*, *103*(3), 1922-1934.

Lozos, J. C., Oglesby, D. D., Brune, J. N., & Olsen, K. B. (2015). Rupture propagation and ground motion of strike-slip stepovers with intermediate fault segments. *Bulletin of the Seismological Society of America*, *105*(1), 387-399.

Madariaga, R. (1977). High-frequency radiation from crack (stress drop) models of earthquake faulting. *Geophysical Journal International*, *51*(3), 625-651.

Oglesby, D. (2008). Rupture termination and jump on parallel offset faults. *Bulletin of the Seismological Society of America*, *98*(1), 440-447.

Okubo, K., Bhat, H. S., Rougier, E., Marty, S., Schubnel, A., Lei, Z., Knight, E., & Klinger, Y. (2019). Dynamics, radiation, and overall energy budget of earthquake rupture with coseismic off-fault damage. *Journal of Geophysical Research: Solid Earth*, *124*(11), 11771-11801.

Oth, A., Miyake, H., & Bindi, D. (2017). On the relation of earthquake stress drop and ground motion variability. *Journal of Geophysical Research: Solid Earth*, *122*(7), 5474-5492.

Savage, J. C. (1965). The stopping phase on seismograms. *Bulletin of the Seismological Society of America*, *55*(1), 47-58.

Shi, Z., & Day, S. M. (2013). Rupture dynamics and ground motion from 3-D rough-fault simulations. *Journal of Geophysical Research: Solid Earth*, *118*(3), 1122-1141.

Sleep, N. H., & Hough, S. E. (2020). Mild Displacements of Boulders during the 2019 Ridgecrest Earthquakes. *Bulletin of the Seismological Society of America*, *110*(4), 1579-1588.

Teran, O., J., Fletcher, J. M., Oskin, M.E., Rockwell, T. K., Hudnut, K. W., Spelz, R. M., Akciz, S. O., Hernandez-Flores, A. P., & Morelan, A.E. (2015). Geologic and Structural controls on rupture zone fabric: A field-based study of the 2010 Mw 7.2 El Mayor Cucapah earthquake surface rupture. *Geosphere*, v. 11, no. 3, p. 899-920.

Wang, K., Dreger, D. S., Tinti, E., Bürgmann, R., & Taira, T. A. (2020). Rupture process of the 2019 Ridgecrest, California M w 6.4 foreshock and M w 7.1 earthquake constrained by seismic and geodetic data. *Bulletin of the Seismological Society of America*, *110*(4), 1603-1626.

Wei, S., Fielding, E., Leprince, S., Sladen, A., Avouac, J. P., Helmberger, D., Hauksson, E., Chu, R., Simons, M., Hudnut, K., Herring, T., & Briggs, R. (2011). Superficial simplicity of the 2010 El Mayor–Cucapah earthquake of Baja California in Mexico. *Nature geoscience*, *4*(9), 615-618.

Wesnousky, S. G. (2008). Displacement and geometrical characteristics of earthquake surface ruptures: Issues and implications for seismic-hazard analysis and the process of earthquake rupture. *Bulletin of the Seismological Society of America*, *98*(4), 1609-1632.

Zuckerman, M., Amos, C., Madugo, C., Elliott, A., Kottke, A., Goulet, C., Meng, X., & Caplan-Auerbach, J (2019, September). Displaced rocks as an indicator of ground motion during the 4 July 2019 M6.4 Ridgecrest earthquake. In *2019 SCEC Annual Meeting Proceedings & Abstracts, XXVIV, poster*.